Synaptic Polarity Depends on Phosphatidylinositol Signaling Regulated by *myo*-Inositol Monophosphatase in *Caenorhabditis elegans*

Tsubasa Kimata,* Yoshinori Tanizawa,* Yoko Can,* Shingo Ikeda,* Atsushi Kuhara,*,[1] and Ikue Mori*,†,[2]
*Laboratory of Molecular Neurobiology, Division of Biological Science, Graduate School of Science, Nagoya University, Nagoya 464-8602, Japan and †Core Research for Evolutional Science & Technology (CREST), Tokyo 102-0075, Japan

ABSTRACT Although neurons are highly polarized, how neuronal polarity is generated remains poorly understood. An evolutionarily conserved inositol-producing enzyme *myo*-inositol monophosphatase (IMPase) is essential for polarized localization of synaptic molecules in *Caenorhabditis elegans* and can be inhibited by lithium, a drug for bipolar disorder. The synaptic defect of IMPase mutants causes defects in sensory behaviors including thermotaxis. Here we show that the abnormalities of IMPase mutants can be suppressed by mutations in two enzymes, phospholipase Cβ or synaptojanin, which presumably reduce the level of membrane phosphatidylinositol 4,5-bisphosphate (PIP_2). We also found that mutations in phospholipase Cβ conferred resistance to lithium treatment. Our results suggest that reduction of PIP_2 on plasma membrane is a major cause of abnormal synaptic polarity in IMPase mutants and provide the first *in vivo* evidence that lithium impairs neuronal PIP_2 synthesis through inhibition of IMPase. We propose that the PIP_2 signaling regulated by IMPase plays a novel and fundamental role in the synaptic polarity.

NEURONS ensure polarized information flows with their diverse morphology. A typical mammalian neuron receives synaptic inputs at branching dendrites and sends signals through a long projecting axon. It has been shown that phosphoinositides, which are derived from combinational phosphorylation of phosphatidylinositol (PI), play important roles in neuronal polarity (Arimura and Kaibuchi 2005; Arimura and Kaibuchi 2007; Skwarek and Boulianne 2009). PI is synthesized from *myo*-inositol, which is supplied by uptake from the extracellular environment, *de novo* synthesis from glucose, or recycling from phosphoinositides (Figure 3B; Agam *et al.* 2009). Of these, the *de novo* synthesis and recycling pathways require *myo*-inositol monophosphatase (IMPase), an evolutionarily conserved enzyme that produces inositol by dephosphorylating inositol monophosphate (Figure 3B; Agam *et al.* 2009).

The *in vivo* function of IMPase has been extensively explored because of its sensitivity to lithium, a drug for bipolar disorder (Cade 1949). Despite the clinical usage for more than half of a century, how lithium exerts its therapeutic effect in patient brains is still enigmatic. Currently, a dominant explanation for the action of lithium is exemplified by the "inositol depletion hypothesis." This hypothesis, mainly based on *in vitro* studies, holds that IMPase inhibition by lithium limits production of inositol, thereby dampening phosphatidylinositol 4,5-bisphosphate (PIP_2)-mediated signaling (Supporting Information, Figure S2; Berridge *et al.* 1982; Berridge *et al.* 1989; Schloesser *et al.* 2008; Machado-Vieira *et al.* 2009). Although it has been shown that lithium inhibits IMPase (Hallcher and Sherman 1980; Hedgepeth *et al.* 1997) and reduces inositol levels (Maslanski *et al.* 1992; O'donnell *et al.* 2000), whether the reduction of inositol affects neuronal PIP_2 levels *in vivo* has been disputed (Batty and Downes 1994; Dixon *et al.* 1994; Berry *et al.* 2004; Schloesser *et al.* 2008; King *et al.* 2009; Machado-Vieira *et al.* 2009). The oppositions to the hypothesis are mainly based on two reasons. First, since inositol can be supplied from the extracellular environment independently

doi: 10.1534/genetics.111.137844
Manuscript received December 14, 2011; accepted for publication March 6, 2012
Available freely online through the author-supported open access option.
Supporting information is available online at http://www.genetics.org/content/suppl/2012/03/23/genetics.111.137844.DC1.
[1]Present address: Laboratory of Molecular Cell Regulation, Department of Biology, Faculty of Science and Engineering, Konan University, Higashinada-ku, Kobe 658-8501, Japan.
[2]Corresponding author: Laboratory of Molecular Neurobiology, Department of Mol Biology, Nagoya University, Nagoya, 464-8602 Japan E-mail: m46920a@nucc.cc.nagoya-u.ac.jp

of IMPase, inhibition of IMPase by lithium might cause only a marginal reduction in the inositol level, which might not substantially impair the synthesis of PI (Batty and Downes 1994; Berry *et al.* 2004). Second, since inhibition of IMPase might alter the levels of inositol polyphosphates that are important regulators of gene expression *in vivo* (Odom *et al.* 2000; Shaldubina *et al.* 2002; Seeds *et al.* 2005; Lee *et al.* 2007), lithium could exert its effect by interfering with these PI-independent metabolic pathways. Thus, it remains unclear how lithium exerts its effect *in vivo*.

We previously reported that the *ttx-7* gene, the *Caenorhabditis elegans* ortholog of IMPase, is required for sensory behaviors. The behavioral defects of *ttx-7* mutants result from abnormality in polarized localization of both pre- and postsynaptic proteins in the interneuron named RIA (Tanizawa *et al.* 2006). The exogenous application of lithium to wild-type animals elicited both the synaptic and behavioral defects similar to those in *ttx-7* mutants (Tanizawa *et al.* 2006), suggesting that lithium inhibits the *C. elegans* IMPase. However, it remains unknown how the inhibition of IMPase leads to such defects.

In this study, we conducted a genetic suppressor screen for *ttx-7* mutants. We found that mutations in the gene *egl-8*, which encodes a homolog of phospholipase Cβ (PLCβ) (Lackner *et al.* 1999; Miller *et al.* 1999), strongly suppress both the synaptic and behavioral defects of *ttx-7* mutants. Since PLCβ cleaves PIP_2, this observation suggests that the accumulation of PIP_2 corrected the defects. Indeed, through screening for known inositol metabolic genes, we found that a mutation in the *unc-26* gene, a homolog of human synaptojanin 1 that dephosphorylates PIP_2 (Cremona *et al.* 1999; Harris *et al.* 2000), also suppresses the synaptic defect in *ttx-7* mutants. Further, *egl-8* mutants showed strong resistance to the lithium treatment. Thus, these results provide the first genetic evidence that disruption of IMPase by lithium affects PIP_2 levels in neurons of living animals and suggest that the PIP_2 signaling establishes polarized localization of pre- and postsynaptic components *in vivo*.

Materials and Methods

Strains and genetics

C. elegans cultures were maintained essentially as described (Brenner 1974). The following strains were used: wild-type Bristol strain (N2), wild-type Hawaiian strain (CB4856) for mapping with snip-SNPs method (Wicks *et al.* 2001), CB47 *unc-11(e47)* I, EG3361 *gqIs25*[*rab-3p*::*ppk-1*, *lin-15*(+)] I, IK575 *ttx-7(nj40)* I, IK589 *ttx-7(nj50)* I, IK685 *njIs20[glr-3p*::*syd-2*::*gfp*, *rol-6gf]* I, IK765 *njIs16[glr-3p*::*eat-4*::*gfp*, *glr-3p*::*snb-1*::*dsredmonomer*, *rol-6gf]* I, CB1265 *unc-104*(*e1265*) II, CB205 *unc-26(e205)* IV, IK661 *njIs9[glr-3p*::*snb-1*::*venus*, *ofm-1p*::*gfp]* IV, IK718 *njIs12[glr-3p*::*glr-1*::*gfp*, *ges-1p*::*Dsredmonomer]* V, IK777 *egl-8(nj77)* V, MT1083 *egl-8(n488)* V, and multiple mutants or transgenic strains generated form them. The rest of strains used are listed in Table 1.

Behavioral assay

The population thermotaxis assay was performed as previously reported (Ito *et al.* 2006) except for Figure S3, F–G, in which the assay duration was 120 min. The individual thermotaxis assay was performed as described (Mori and Ohshima 1995). The salt chemotaxis assay was performed as described (Komatsu *et al.* 1996).

Genetic screens for mutations that suppress thermotaxis defects of ttx-7 mutants

ttx-7(*nj40*) animals were mutagenized with ethyl methanesulfonate (EMS) as described before (Brenner 1974), and F_1 progeny was isolated to 6-cm NGM plates. F_2 progeny from five F_1 plates was cultured at 23° and was assayed in the population thermotaxis assay for 40 min. *egl-8(nj77)* was isolated as animals that migrated to 23°.

Mapping of nj77

We outcrossed *ttx-7*(*nj40*) to CB4856 to generate the strain carrying *ttx-7*(*nj40*) in a Hawaiian background. By utilizing the SNPs (single nucleotide polymorphisms) between this strain and the suppressor, we mapped *nj77* to a 1 Mbp region of the left end of chromosome V.

Molecular biology

An *egl-8 cDNA* (KP316) is a gift from Dr. Stephan Nurrish. The promoter of the *glr-3* gene was used as an RIA-specific promoter. To generate *glr-3p*::*egl-8* cDNA (pUBA13), the *egl-8* cDNA was amplified by PCR from KP316 plasmid, and the *ttx-7a* cDNA::*egfp* of *glr-3p*::*ttx-7a* cDNA::*egfp* (pTAN58) was replaced by the *egl-8* cDNA. To generate *glr-3p*::*gfp*::*egl-8* cDNA (pUBA21), an *gfp*::*egl-8* cDNA was amplified by PCR from *acr-2p*::*gfp*::*egl-8* cDNA (REW1) plasmid, and the *ttx-7a* cDNA::*egfp* of *glr-3p*::*ttx-7a* cDNA::*egfp* (pTAN58) was replaced by the *gfp*::*egl-8* cDNA. To generate *glr-3p*::*unc-101* cDNA::*egfp* (pUBA35), a *unc-101* cDNA was amplified from *C. elegans* yeast two-hybrid cDNA library (Cosmo Bio Co., Ltd), and the *ttx-7a* cDNA of *glr-3p*::*ttx-7a* cDNA::*egfp* (pTAN58) was replaced by the *unc-101* cDNA

Transgenic animals

Germline transformation was performed by co-injecting experimental DNA (1–100 ng/μl) and an injection marker pKDK66 (*ges-1p*::*NLS*::*GFP*), *ofm-1*::*gfp*, pRF4 (*rol-6gf*), or pTAN124.5 (*ges-1p*::*Dsredmonomer*) (Mello *et al.* 1991). Multiple independent transgenic lines were established for each experimental DNA. For comparison of phenotypes on different genetic backgrounds, transgenic arrays were transferred by intercrossing. Strains with integrated arrays were established by TMP/UV mutagenesis of animals carrying an extrachromosomal array as described (Tanizawa *et al.* 2006).

Lithium treatment

Animals were cultivated on LiCl-containing NGM plates from birth. LiCl (Wako) was added at 15 mM concentration

Table 1 Localizarion of SNB-1 in mutants related to neuronal polarity, synapse formation, or inositol metabolism

Strain used	Mutation	Gene	Localization of snb-1
N2	Wild type	—	Presynaptic region
IK589	*ttx-7(nj50)*	IMPase	Entire process
	Polarity- or synapse-related genes		
KU17	*lrk-1(km17)*[a]	LRRK2/PARK8-related kinase	WT
VC898	*cdc-42(gk388)*[b,c]	Cdc42	WT
NG324	*wsp-1(gm324*[b]	WASP	WT
VC2053	*wip-1(ok2435)*[b,c]	WASP-interacting protein	WT
VC2706	*wve-1(ok3308)*[b,c]	WAVE	WT
DR1	*unc-101(m1)*	AP-1 medium subunit	WT
DR1	*ttx-7(nj40) unc-101(m1)*	AP-1 medium subunit	*ttx-7*-like
CB1193	*unc-33(e1193)*	CRMP	WT
CB204	*unc-33(e204)*	CRMP	WT
SP1382	*unc-33(mn407)*	CRMP	WT
EM67	*mab-20(bx24)*[a]	Semaphorin-2A	WT
CB78	*unc-6(e78)*[a]	Netrin	WT
CB271	*unc-40(e271)*[a]	Netrin receptor	WT
CB362	*unc-44(e362)*[b]	Ankyrin G	WT
	Inositol metabolism-related genes		
CB205	*unc-26(e205)*	Synaptojanin	WT (Figure 4)
CB205	*ttx-7(nj50);unc-26(e205)*	Synaptojanin	WT (Figure 4)
RB1535	*arf-1.1(ok1840)*	ADP-ribosylation factor family	WT
VC567	*arf-1.2(ok796)*	ADP-ribosylation factor family	WT
FX1447	*arf-6(tm1447)*[b]	ADP-ribosylation factor family	WT
KU22	*pld-1(km22)*	Phospholipase D	WT
VC1587	*ocrl-1(gk752)*	OCRL	WT
VC1587	*ttx-7(nj40) ocrl-1(gk752)*	OCRL	*ttx-7*-like
IK1130	*age-1(mg305)*	Phosphoinositide 3-kinase	WT
IK1130	*ttx-7(nj50);age-1 (mg305)*	Phosphoinositide 3-kinase	*ttx-7*-like
RB1813	*piki-1(ok2346)*	Phosphoinositide 3-kinase	WT
KR1440	*vps-34(h797)*[b,c]	Phosphoinositide 3-kinase	WT
FX2348	*F35H12.4(tm2348)*[b]	Phosphatidylinositol kinase	WT
VC2563	*Y75B8A.24(ok3320)*[b]	Phosphatidylinositol kinase	WT
EG3361	*ttx-7(nj50) gpIs25[rab-3p::ppk-1]*	Type I PI-4-phosphate kinase	*ttx-7*-like
FX3741	*ppk-2(tm3741)*[b]	Type II PI -5-phosphate kinase	WT
MT7531	*ppk-3(n2835)*[b]	Type III PI-3-phosphate kinase	WT
MT12352	*trr-1(n3630)*[b,c]	TRAAP subfamily	WT
TR1331	*smg-1(r861)*[b]	Phosphatidylinositol kinase	WT
VC381	*atm-1(gk186)*[b]	ATM family	WT
VC728	*atl-1(ok1063)*[b]	ATM family	WT
VC2312	*let-363(ok3013)*[b,c]	FRAP1	WT
FX753	*plc-1(tm753)*	Phospholipase c	WT
FX753	*ttx-7(nj40);plc-1 (tm753)*	Phospholipase c	*ttx-7-like*
RB1496	*plc-2(ok1761)*[b]	Phospholipase c	WT
RB1496	*ttx-7(nj50);plc-2(ok1761)*[b]	Phospholipase c	*ttx-7*-like
MT1434	*egl-30(n686)*	G-protein α-subunit	WT
KY26	*egl-30(tg26gf)*	G-protein α-subunit	WT
MT1434	*egl-30(n686) ttx-7(nj50)*	G-protein α-subunit	*ttx-7*-like

Localization of SNB-1 in RIA neuron was examined. About 10 adult animals were examined in more than three trials for each genotype. In the mutants without the superscripts, the localization of SNB-1::VENUS expressed from integrated array was observed. WT and *ttx-7*-like represents the wild-type and *ttx-7*-like mutant phenotypes of SNB-1 localization, respectively.

[a] The localization of SNB-1::DsRedmonomer expressed from integrated array was observed.

[b] The localization of SNB-1::VENUS expressed from extrachromosomal array was observed.

[c] These mutants display larval arrest or developmental defects. The localization of SNB-1 in these mutants was examined at larval stages; SNB-1 localized to the distal region of the process in wild-type animals at laval stages as well as at the adult stage.

to NGM medium. We used 1-day-old adults for phenotypic analyses.

Observation and quantification of synaptic molecule localization

An Axioplan2 light microscope (Zeiss) was used to observe the synaptic molecule localization. The fluorescent images were captured with a confocal laser-scanning microscope FV1000 (Olympus). The quantifications of localization indices for SNB-1::VENUS, GFP::SYD-2, and GLR-1::GFP were performed on adult animals with integrated arrays. The localization index was calculated using ImageJ software (NIH): the area and mean fluorescence intensity of the background, presynaptic region (region A), and non-presynaptic

region (region B) of the RIA process (Figure 2B) were measured for each slice of a confocal image. The total intensity in each region for each slice was generated by subtracting the mean intensity of the background from that of the region of interest, which was then multiplied by its area. The fluorescence of the region A and B was calculated by summing the total intensity of each slice of each region. The localization index was calculated as fluorescence A / fluorescence A + B.

Statistics

Error bars in all figures indicate standard error of the mean (SEM). We treated thermotaxis indices and localization indices as parametric and nonparametric data, respectively. The comparison test methods applied are indicated in each figure legend. The double asterisks (**), single asterisks (*), and no significances (NS) in all figures represent $P < 0.01$, $P < 0.05$, and $P > 0.05$, respectively.

Results

A mutation in the egl-8 gene strongly suppresses the behavioral abnormalities of ttx-7 mutants

The *ttx-7* gene encodes the sole ortholog of IMPase gene in *C. elegans*. Tanizawa *et al.* (2006) showed that the loss of TTX-7 causes defects in both polarized distribution of synaptic proteins in the RIA interneuron and behaviors including thermotaxis (Tanizawa *et al.* 2006). Thermotaxis is one of the most characterized experience-dependent behaviors in *C. elegans*: when well-fed animals cultivated at a certain temperature are placed on a temperature gradient (shallower than 1°/cm) without food, they migrate toward their cultivated temperatures and move isothermally (Hedgecock and Russell 1975; Mori and Ohshima 1995; Mohri *et al.* 2005; Jurado *et al.* 2010). RIA receives synaptic inputs from upstream interneurons in the neural circuit regulating thermotaxis (Figure S1A; Mori and Ohshima 1995). Since RIA neuron-specific expression of *ttx-7* cDNA rescued both the synaptic and thermotaxis defects, abnormal thermotaxis phenotype of *ttx-7* mutants is likely caused by synaptic defects in RIA (Tanizawa *et al.* 2006).

To clarify further how IMPase regulates the synaptic polarity and consequently sensory behaviors, we conducted a genetic suppressor screen for *ttx-7* mutants utilizing a population thermotaxis assay (*Materials and Methods*). Of five isolates among ~2000 genomes screened in a *ttx-7(nj40)* background, we focused on the mutation *nj77* that strongly suppressed the thermotaxis defect.

The snip-SNPs method (Wicks *et al.* 2001) and subsequent sequencing analyses revealed a G-to-A mutation in the splicing donor site of the eighth intron of the *egl-8* gene in the *nj77* mutant genome (Figure 3A). The *egl-8* gene encodes a homolog of PLCβ, most closely related to PLCβ4 in vertebrates (Lackner *et al.* 1999; Miller *et al.* 1999). *ttx-7 (nj40);nj77* mutants showed slightly flattened sinusoidal tracks on cultivation plates unlike *ttx-7(nj40)* single mutants, which are characteristic of *egl-8* mutant animals (data not shown; Lackner *et al.* 1999). RIA-specific expression of *egl-8* cDNA abolished the suppressible effect of *nj77* mutation (Figure 3D and Figure S1D; discussed below). These results indicate that *nj77* is an allele of *egl-8*.

We further analyzed the thermotaxis behavior of *ttx-7; egl-8(nj77)* mutants, using a deletion or a hypomorphic allele, *ttx-7(nj50)* or *ttx-7(nj40)*, respectively. To investigate the ability of migrating toward cultivation temperature on a thermal gradient, we utilized the population thermotaxis assay (Figure 1A; Ito *et al.* 2006). After cultivation at 23°, 20°, or 17° in a well-fed condition, most wild-type animals migrated toward their cultivation temperatures, whereas *ttx-7* mutants dispersed on the assay plate (Figure 1B and Figure S1B). In contrast, *ttx-7;egl-8(nj77)* mutants migrated toward their cultivation temperatures. *ttx-7;egl-8(nj77)* and *egl-8(nj77)* single mutants accumulated at the temperature slightly higher or lower than wild-type animals in 17° or 23° cultivation, respectively (Figure 1B and Figure S1B). Since animals carrying a deletion allele of *egl-8*, *egl-8(n488)*, do not move on the assay plate owing to locomotion defects (Okochi *et al.* 2005), the thermotaxis abnormalities in *ttx-7; egl-8(nj77)* and *egl-8(nj77)* mutants might be caused by a defect in locomotion. To test this possibility, we assayed wild-type and *egl-8(nj77)* mutant animals cultivated at 17° or 23° on the assay plates without the temperature gradient and compared the TTX deviations, which reflect the dispersion of the animals (Figure S3A; Ito *et al.* 2006). The TTX deviations between wild-type and *egl-8(nj77)* mutants were not considerably different (Figure S3, B–E). We found that extending the assay duration from 60 to 120 min improved the thermotaxis performance of *egl-8(nj77)* mutants cultured at 17° but not at 23° (Figure S3, F and G). These results suggest that *egl-8* is involved in thermotaxis rather than merely affecting the locomotion.

After reaching the cultivation temperature, animals move isothermally (IT behavior) (Hedgecock and Russell 1975; Mori and Ohshima 1995; Ryu and Samuel 2002; Luo *et al.* 2006). Since RIA is essential for IT behavior (Figure S1A; Ohnishi *et al.* 2010), we tested this behavior using the individual thermotaxis assay with a radial temperature gradient (Mori and Ohshima 1995). In contrast to wild-type animals showing clear isotherms, *ttx-7* mutants moved almost randomly on the gradient (Figure 1, D and E). By contrast, *ttx-7;egl-8(nj77)* double mutants showed IT behavior similar to those of wild-type animals and *egl-8(nj77)* single mutants (Figure 1, D and E), suggesting that *egl-8 (nj77)* restores the function of RIA in *ttx-7* mutants.

ttx-7 mutants was previously shown to be defective in salt attraction (Figure 1C; Tanizawa *et al.* 2006). We found that *ttx-7(nj50);egl-8(nj77)* and *egl-8(nj77)* mutants were attracted to NaCl to the similar extent to that of wild-type animals (Figure 1C). Taken together, we concluded that *egl-8(nj77)* confers strong suppression for the behavioral defects of *ttx-7* mutants.

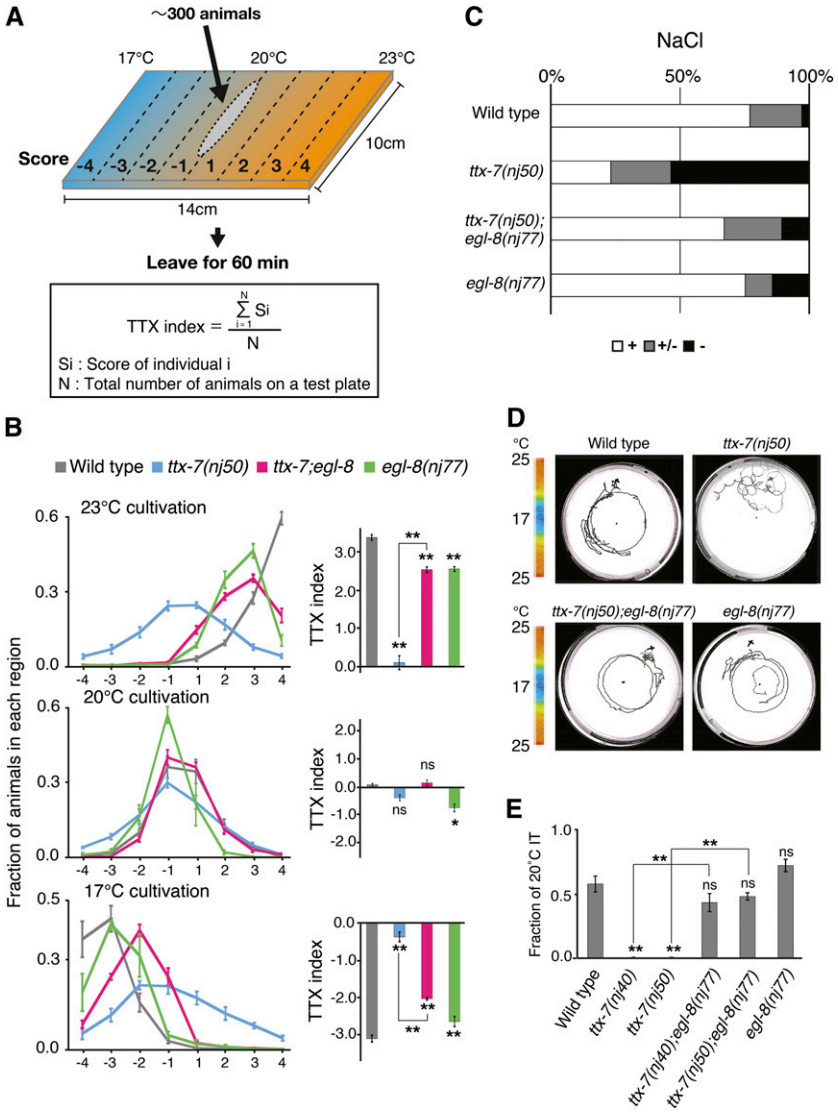

Figure 1 Behavior of *ttx-7;egl-8* double mutants. (A) Procedure for the population thermotaxis assay. Between 50 and 300 animals cultivated at a certain temperature were placed at the center of the liner temperature gradient ranging from 17° to 23° in 14 cm width. After 60 min, the number of animals at each region was counted. The TTX index was calculated using the equation shown here. (B) Distributions and TTX indices of animals cultivated at 17°, 20°, and 23°. While *ttx-7(nj50)* mutants showed almost athermotactic behavior, *ttx-7(nj50);egl-8(nj77)* double mutants migrated toward the cultivation temperatures. Tukey–Kramer test was applied ($n \geq 4$ assays). The marks on the bars of each genotype represent comparisons with wild type. The marks on the lines represent comparisons between indicated genotypes. (C) Individual chemotaxis assay to NaCl. (+) strong attraction; (+/−) modest attraction; (−) no attraction to NaCl. *egl-8 (nj77)* strongly suppressed the chemotaxis defect of *ttx-7(nj50)* mutants. n ≥ 57 animals. (D) Individual thermotaxis assay of animals cultivated at 20°. The center and edge of the 9-cm plate are maintained at 17° and 25°, respectively. In contrast to the random movement of *ttx-7(nj50)* mutants, *ttx-7(nj50);egl-8 (nj77)* mutants showed clear isothermal tracking (IT) around 20° as well as wild-type animals. (E) Fraction of animals that moved isothermally around 20° in the individual thermotaxis assay. *nj40* and *nj50* are hypomorphic and putative null alleles for *ttx-7*, respectively. *egl-8(nj77)* strongly suppressed the defect of *ttx-7* mutants. About 20 animals were examined in more than three trials, which were compared in ANOVA. The marks on the bars of each genotype indicate comparisons with wild type. The marks on the lines represent comparisons between indicated genotypes.

Loss of EGL-8 suppresses the synaptic defects of ttx-7 mutants

We next addressed whether *egl-8* mutations also suppress the synaptic defects of *ttx-7* mutants. The RIA interneuron has a single process where pre- and postsynaptic regions are segregated, providing a unique platform from which to analyze the polarized distribution of synaptic proteins *in vivo* (Figure 2, A and B; White *et al.* 1986; Tanizawa *et al.* 2006; Margeta *et al.* 2009). The localization of fluorescent marker-tagged synaptic proteins in the process was evaluated using the "localization index" shown in Figure 2B. The synaptic vesicle-associated protein SNB-1 fused to VENUS was exclusively localized to the presynaptic region of RIA in wild-type and *egl-8* mutant animals (Figure 2, C, F, and G). As previously reported, SNB-1::VENUS was abnormally localized in both pre- and nonpresynaptic regions of the RIA process in *ttx-7* mutants (Figure 2, C, F, and H; Tanizawa *et al.* 2006), whereas both *egl-8(nj77)* and *egl-8(n488)* markedly suppressed the localization defect of *ttx-7* mutants (Figure 2, C, F, and G). We noted that the suppression by *egl-8(nj77)* was weaker than *egl-8(n488)* ($P < 0.01$: comparison between *nj50;nj77* and *nj50;n488* in Figure 2C). This result and the locomotion phenotype described above suggest that *nj77* is a hypomorphic allele of *egl-8*. We next examined the localization of SYD-2, a presynaptic active zone protein (Yeh *et al.* 2005). The SYD-2 tagged with GFP was mainly localized to the presynaptic region in wild-type and *egl-8* mutant animals, whereas in *ttx-7* mutants, the fluorescent puncta in the presynaptic region was dispersed throughout the whole process (Figure 2, D, F, I, and J; Tanizawa *et al.* 2006). As in the case of SNB-1, *egl-8*(*n488*) strongly suppressed this defect (Figure 2, D, F, and I).

We also examined postsynaptic specializations using GLR-1, an AMPA-type glutamate receptor. The GLR-1::GFP was localized to the postsynaptic region in wild-type and *egl-8* mutant animals, while it diffused throughout the entire process in *ttx-7* mutants (Figure 2, E, F, K and L; Tanizawa *et al.* 2006). *egl-8*(*n488*) completely suppressed this defect

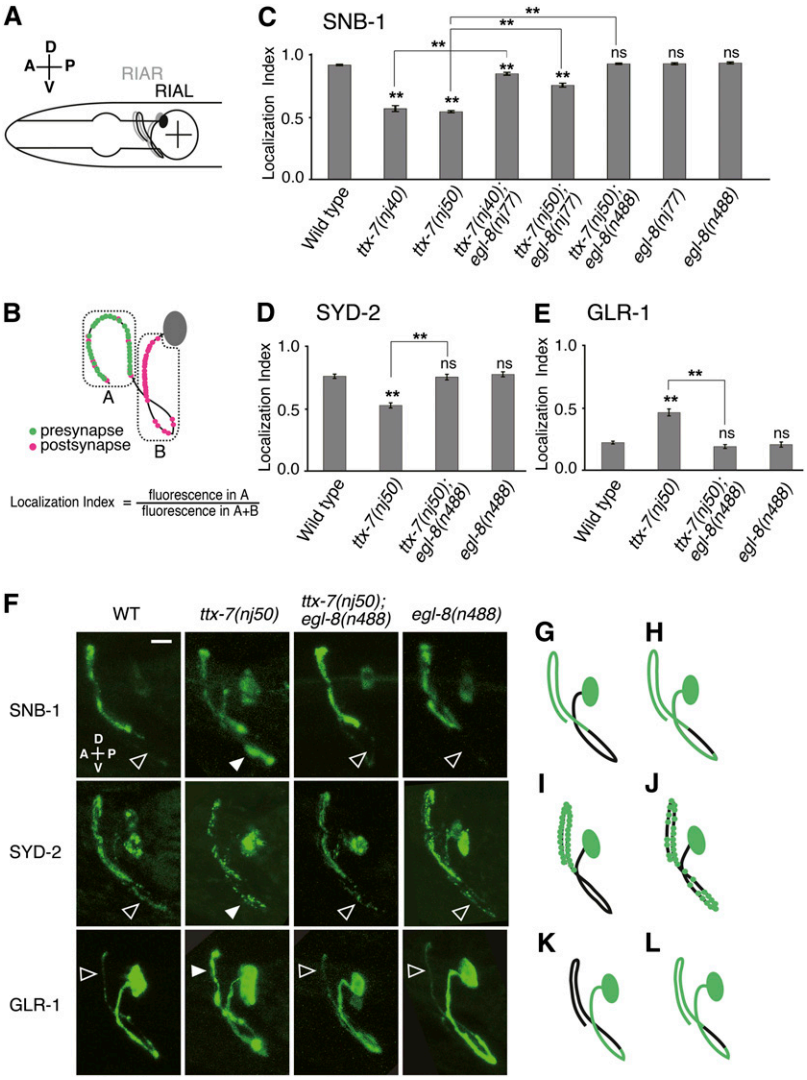

Figure 2 Mutations in *egl-8* strongly suppress the synaptic defects of *ttx-7* mutants. (A) Schematic of the head region of *C. elegans* and a pair of RIA. (B) Schematic of pre- and postsynapses distribution in RIA (White *et al.* 1986). The localization index was calculated using the equation shown here. Measurement of fluorescent intensity was performed as described in *Materials and Methods*. (C–E) Comparison of the localization indices of SNB-1::VENUS (C), GFP::SYD-2 (D), and GLR-1::GFP (E) in the RIA neuron in each genotype. Mutations in *egl-8* strongly suppressed the localization defects of the synaptic proteins in *ttx-7* mutants. Note that *egl-8(n488)* suppressed more strongly than *egl-8(nj77)* (C). Steel–Dwass multiple comparison tests were performed ($n \geq 11$ animals). The marks on the bars of each genotype indicate comparisons with wild type. The marks on the lines indicate comparisons between indicated genotypes. (F) Representative images of the distribution of each synaptic protein in the RIA neuron in each genotype. Solid arrowheads indicate ectopic fluorescence, and open arrowheads indicate absence of the ectopic fluorescence. Scale bar, 5 μm. (G and H) Schematic of SNB-1::VENUS localization in wild-type animals, *ttx-7(nj50);egl-8(n488)* and *egl-8(n488)* mutants (G) and that in *ttx-7(nj50)* mutants (H). SNB-1::VENUS is mislocalized at the proximal region of the process in *ttx-7(nj50)* mutants. (I and J) Schematic of GFP::SYD-2 localization in wild-type animals, *ttx-7(nj50);egl-8(n488)* and *egl-8(n488)* mutants (I) and that in *ttx-7(nj50)* mutants (J). GFP::SYD-2 mainly localized to the distal region of RIA in wild-type animals, *ttx-7(nj50); egl-8(n488)* and *egl-8(n488)* mutants, while it dispersed in whole process in *ttx-7(nj50)* mutants. (K and L) Schematic of GLR-1::GFP localization in wild-type animals and *ttx-7 (nj50);egl-8(n488)* and *egl-8(n488)* mutants (K) and that in *ttx-7(nj50)* mutants (L). GLR-1::GFP mainly localized in the proximal region of RIA in wild-type animals, *ttx-7(nj50); egl-8(n488)* and *egl-8(n488)* mutants, while it diffused in whole process in *ttx-7(nj50)* mutants.

(Figure 2, E, F and K). These results indicate that *egl-8* mutations confer the strong suppression for the synaptic defects in *ttx-7* mutants.

Disruption of EGL-8-mediated PIP_2 degradation in RIA suppresses the abnormalities in ttx-7 mutants

To examine where the *egl-8* gene acts, we conducted cell-specific rescue experiments. The RIA-specific expression of *egl-8* cDNA in *ttx-7;egl-8* double mutants substantially reduced the fraction of IT behavior (Figure 3D and Figure S1D), and also disrupted localizations of SNB-1 and SYD-2 similarly to *ttx-7* single mutants (Figure 3, E and F, and Figure S4D). These results indicate that the loss of *egl-8* function in RIA restores the abnormalities in *ttx-7* mutants.

egl-8 encodes PLCβ that hydrolyzes PIP_2 on plasma membrane (Figure 3B; Lackner *et al.* 1999; Miller *et al.* 1999). Because local PI metabolism on cell membrane is thought to be important for polarity establishment (Skwarek and Boulianne 2009), we assessed whether the PIP_2 hydrolysis is restricted to a domain(s) of the RIA process such as pre- and postsynaptic domains by examining the subcellular localization of EGL-8. A functional GFP::EGL-8 (Figure S1C) was diffusely localized presumably on the membrane of the entire process and cell body (Figure 3C). This result suggests that PIP_2 hydrolysis is not restricted to any specific regions of the RIA process but does not exclude the possibility that EGL-8 activity is spatially restricted by a regulator protein. Given that EGL-8 is activated by the G-protein α-subunit EGL-30 at neuromuscular junctions (Lackner *et al.* 1999; Miller *et al.* 1999), we speculated that EGL-30 also regulates EGL-8 in RIA. However, we did not see the clear suppression of the defective localization of SNB-1::VENUS in *ttx-7(nj50); egl-30(n686)* double mutants, and gain- or loss-of-function mutations in *egl-30* did not cause localization defects (Table 1). It is still possible that a protein different from EGL-30 regulates the activity of EGL-8 in RIA.

Screening for PI metabolic genes regulating the localization of synaptic components

The loss of EGL-8/PLCβ would cause an increase of PIP_2 and a decrease of IP_3 and DAG (Figure 3B). To test which of these two changes is responsible for the suppression of the

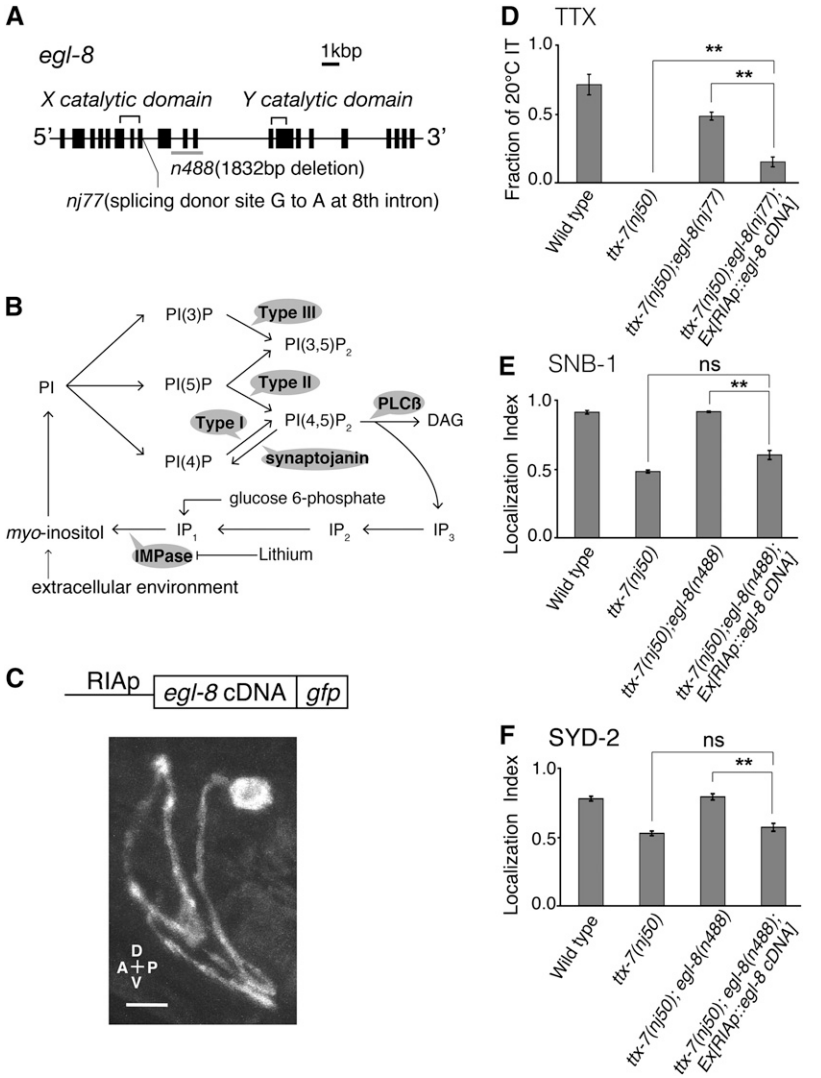

Figure 3 Loss of EGL-8 function in RIA suppresses the abnormalities in *ttx-7* mutants. (A) Locations of *nj77* and *n488* mutations in *egl-8* gene. Solid boxes indicate exons. (B) Simplified model of PI metabolism. *myo*-Inositol is supplied by *de novo* synthesis from glucose 6-phosphate and recycling from phosphoinositides, which require IMPase to dephosphorylate inositol monophosphate (IP_1). *myo*-Inositol is also supplied from the extracellular environment via membrane-associated transporters. PI is synthesized from *myo*-inositol, and type I, II, and III of PIP kinases phosphorylate PI(4)P, PI(5)P, and PI(3)P, respectively. PLCβ cleaves $PI(4,5)P_2$ into DAG and IP_3. IP_3 is sequentially dephosphorylated into *myo*-inositol. Synaptojanin dephosphorylates the five-position phosphate from $PI(4,5)P_2$. IMPase can be inhibited by lithium *in vivo*. (C) The subcellular localization of EGL-8::GFP in the RIA neuron. EGL-8::GFP was not localized to a specific region. Scale bar, 5 μm. (D) Expressing *egl-8* cDNA specifically in RIA reduced the fraction of IT behavior in *ttx-7(nj50);egl-8(nj77)* double mutants. About 20 animals cultivated at 20° were examined in more than three trials, which were compared in ANOVA. (E and F) The localization indices of SNB-1::VENUS (E) and GFP::SYD-2 (F). The RIA-specific expression of *egl-8* cDNA reduced the localization indices in *ttx-7(nj50); egl-8(n488)* double mutants. Steel–Dwass multiple comparison tests were performed ($n \geq 11$ animals).

ttx-7 phenotype, we examined the SNB-1 localization in the RIA neuron of animals mutant for genes involved in PI metabolism (Table 1). First, we examined the gene *unc-26*, encoding a *C. elegans* ortholog of human synaptojanin 1 that regulates the clathrin uncoating step of endocytosis through dephosphorylation of PIP_2 on plasma membrane (Figure 3B; Cremona *et al.* 1999; Harris *et al.* 2000). The *unc-26* mutation substantially suppressed the localization defects of synaptic proteins in *ttx-7* mutants (Figure 4 and Table1). We could not assess the thermotaxis phenotype of *ttx-7(nj50); unc-26(e205)* double mutants owing to locomotion defects. Given that the level of PIP_2 was reported to be selectively increased in neurons of synaptojanin-knockout mice (Cremona *et al.* 1999) and that the loss of *unc-26* would not decrease IP_3 and DAG levels (Figure 3B), our result suggests that accumulation of membrane PIP_2 suppresses the defects of *ttx-7* mutants.

The *ppk-1* gene encodes a type I PIP kinase that is regarded as a primary synthetic enzyme for PIP_2 *in vivo* (Figure 3B; Stephens *et al.* 1991; Whiteford *et al.* 1997; Weinkove *et al.* 2008). Weinkove *et al.* (2008) showed that the overexpression of *ppk-1* under a panneural promoter significantly increases PIP_2 levels, while *ppk-1(ok1141)* mutants display an early larval lethal phenotype (Weinkove *et al.* 2008). We examined whether the overexpression of *ppk-1* suppresses the defects of *ttx-7* mutants. SNB-1::VENUS was still mislocalized in the nonpresynaptic region of RIA in the *ppk-1* overexpression strain with *ttx-7(nj50)* mutation, as observed in *ttx-7(nj50)* single-mutant animals (Figure S4C and Table 1). The *ppk-2* and *ppk-3* genes encode homologs of type II and III PIP kinase, respectively. Type II kinase generates PIP_2, and type III kinase generates phosphatidylinositol 3,5-bisphosphate (Figure 3B; Nicot *et al.* 2006; Weinkove *et al.* 2008). In both mutants, SNB-1::VENUS was normally localized at the presynaptic region (Table 1). In addition, we examined mutants for genes encoding phospholipase D (*pld-1*), ADP-ribosylation factor (*arf-1.1*, *arf-1.2*, *arf-6*), and Lowe oculocerebrorenal syndrome protein (*ocrl-1*). Homologs of these genes are involved in the metabolism of PIP_2 in the Golgi apparatus in

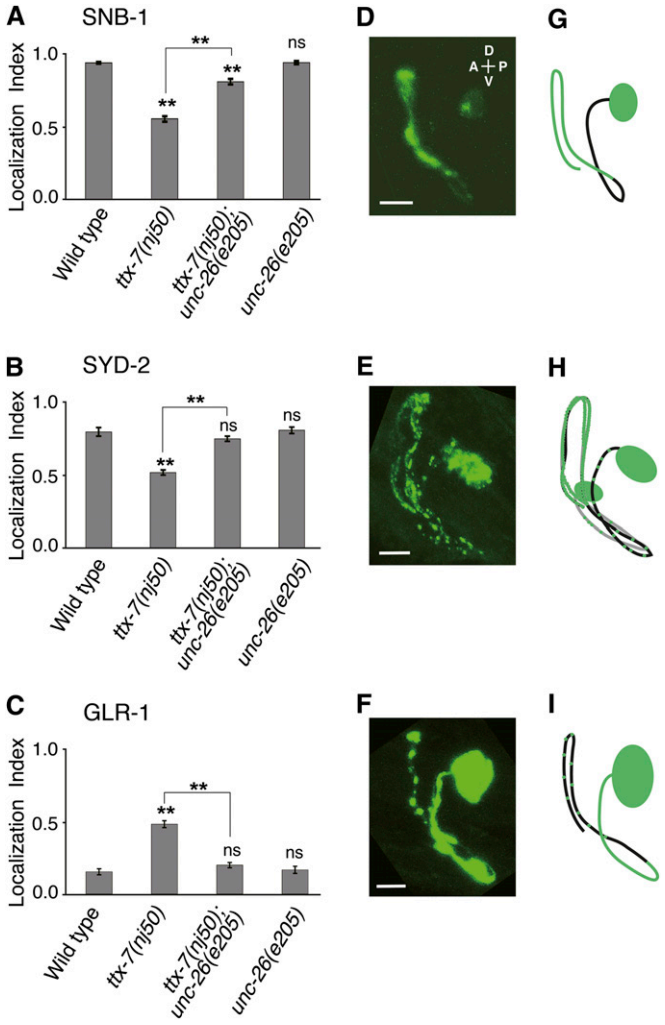

Figure 4 A mutation in the *unc-26* gene suppresses the synaptic defects of *ttx-7* mutants. (A–C) The localization indices of SNB-1::VENUS (A), GFP::SYD-2 (B), and GLR-1::GFP (C). A mutation in *unc-26* significantly suppressed the localization defects of the synaptic proteins in *ttx-7(nj50)* mutants. The marks on the bars of each genotype indicate comparisons with wild type. The marks on the lines indicate comparisons between indicated genotypes. Steel–Dwass multiple comparison tests were performed ($n \geq 11$ animals). (D–F) Representative confocal images of the RIA neuron expressing SNB-1::VENUS (D), GFP::SYD-2 (E), and GLR-1::GFP (F) in *ttx-7(nj50);unc-26(e205)* double mutants. Scale bar, 5 μm. (G–I) Schematics of SNB-1::VENUS (G), GFP::SYD-2 (H), GLR-1::GFP (I) localizations in the RIA neuron of *ttx-7(nj50);unc-26(e205)* double mutants.

mammals (De Matteis *et al.* 2002; Di Paolo and De Camilli 2006). We did not identify any defects in these mutants (Table 1). We also tested mutations in the genes encoding phospholipase C isozymes (*plc-1*, *plc-2*) and proteins with the PI kinase domain (*age-1*, *piki-1*, *vps-1*, F35H12.4, Y75B8A.24, *trr-1*, *smg-1*, *atm-1*, *atl-1*, *let-363*), but these mutations neither caused a *ttx-7*-like defect nor suppressed the defect of *ttx-7* mutants (Table 1). These results suggest that TTX-7 and the PI-related enzymes examined here function in distinct PI metabolic processes.

The synaptic defect in ttx-7 mutants is not merely a reflection of any known defects of polarity genes

The synaptic defects in *ttx-7* mutants might be caused by defects in a selective transport system of synaptic proteins. We tested this possibility with a mutation in LRK-1, a homolog of familial parkinsonism gene PARK8/LRRK2, which causes a defect in the selective transport system, resulting in the abnormal localization of SNB-1 in sensory neurons (Sakaguchi-Nakashima *et al.* 2007). We did not, however, find any mislocalization defects of SNB-1 in the RIA neuron of *lrk-1(km17)* mutants (Table 1). Although the localization defect of SNB-1 in sensory neurons of *lrk-1* mutants is suppressed by the loss of UNC-101 that is required for the transport of postsynaptic proteins (Sakaguchi-Nakashima *et al.* 2007), the mislocalization defect of SNB-1::VENUS in RIA neuron of *ttx-7* mutants was not suppressed by a null mutation in *unc-101* (Table 1; Dwyer *et al.* 2001). These results suggest that the molecular mechanism for the polarized localization of SNB-1 in RIA is different from that in sensory neurons.

Another possibility for the mechanism of the mislocalization is that the physical barriers between subcellular compartments in RIA are broken in *ttx-7* mutants. A recent study revealed that ankyrin G is necessary for the cytosolic filter of axon initial segments (Song *et al.* 2009). We found that mutants for *unc-44* gene encoding a *C. elegans* homolog of ankyrin G (Otsuka *et al.* 1995) showed normal localization of SNB-1::VENUS in RIA (Table 1).

Studies of cultured neurons have identified several molecules needed for cell polarity (Arimura and Kaibuchi 2007; Takenawa and Suetsugu 2007). Of *C. elegans* homologs of these molecules, mutants for cell division control protein 42 (*cdc-42*) (Gotta *et al.* 2001; Kay and Hunter 2001), collapsin response mediator protein-2 (CRMP-2) (*unc-33*) (Tsuboi *et al.* 2005), neural Wiskott–Aldrich syndrome protein (N-WASP) (*wsp-1*), WASP family Verprolin-homologous protein (WAVE) (*wve-1*), and proline-rich WASP-interacting protein (WIP) (*wip-1*) (Sawa *et al.* 2003; Sawa and Takenawa 2006) all showed normal localization of SNB-1::VENUS in the RIA neuron (Table 1). These results suggest that the polarized localization of synaptic molecules in RIA is controlled by a novel mechanism for neuronal polarity.

Mislocalization of synaptic vesicle proteins occurs independently of UNC-104, a kinesin-like protein

Kinesin motor proteins carry motor-specific cargos, assuring selective transport in neurons. UNC-104 is a kinesin-like motor protein and transports synaptic vesicles (SV) in *C. elegans* (Hall and Hedgecock 1991; Otsuka *et al.* 1991). Consistently, the fluorescence of SNB-1::VENUS was observed exclusively in the cell body of RIA in most of *unc-104(e1265)* mutant animals (Figure 5, A, B, and D). We examined whether the mislocalized SNB-1::VENUS in *ttx-7* mutants is transported by UNC-104. We observed

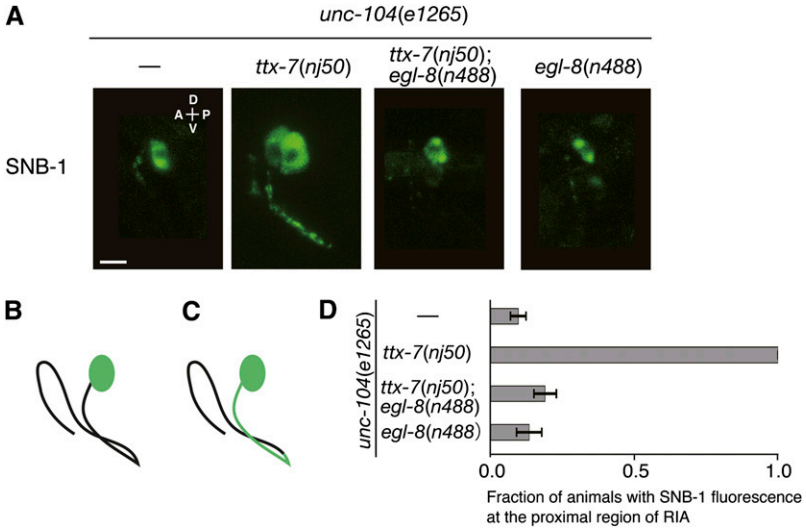

Figure 5 Localization of SNB-1 in a *unc-104*-mutant background. (A) Representative images of SNB-1::VENUS localization in the RIA neuron in each genotype. The fluorescence of SNB-1::VENUS in *unc-104(e1265)*, *ttx-7 (nj50);unc-104(e1265);egl-8(n488)*, and *unc-104(e1265); egl-8(n488)* mutants was localized exclusively in the cell body, while it was abnormally localized as punctate in proximal region of the process in *ttx-7(nj50);unc-104 (e1265)* mutants. Scale bar, 5 μm. (B and C) Schematic of SNB-1::VENUS localization in the RIA neuron of *unc-104(e1265)*, *ttx-7(nj50);egl-8(n488);unc-104(e1265)*, and *egl-8(n488);unc-104(e1265)* mutants (B) and that of *ttx-7(nj50);unc-104(e1265)* mutants (C). (D) The fraction of animals that displayed abnormal localization of SNB-1::VENUS in the proximal region of the RIA process in each genotype. SNB-1::VENUS expressed from integrated array *njIs9* was observed. About 20 animals were examined in more than three trials.

punctate fluorescence in the proximal region of the process in *ttx-7(nj50);unc-104(e1265)* double mutants, although the presynaptic localization of SNB-1::VENUS was abolished (Figure 5, A, C, and D). Further, this abnormal localization of SNB-1::VENUS was suppressed by *egl-8*(*n488*) (Figure 5, A, B, and D). These results suggest that some portion of SNB-1::VENUS is mislocalized by an UNC-104-independent pathway in *ttx-7* mutants. Nonet *et al.* (1999) reported that a mutation in *unc-11* causes diffused localization of SNB-1 in the nerve processes in a *unc-104* background (Nonet *et al.* 1999). We found that the appearance of the SNB-1 fluorescence in *unc-11(e47);unc-104(e1265)* mutants was different from that of *ttx-7(nj50);unc-104(e1265)* mutants (Figure 5A and Figure S4B), suggesting that the losses of UNC-11 and TTX-7 cause mislocalization of SNB-1 in different processes.

egl-8 mutants are resistant to LiCl treatment on synaptic and thermotaxis phenotypes

Lithium is used to treat bipolar disorder, and IMPase is one of the putative targets of lithium therapy (Hallcher and Sherman 1980; Berridge *et al.* 1989). Tanizawa *et al.* (2006) showed that the exogenous application of LiCl to wild-type animals mimics both the thermotaxis and synaptic defects of *ttx-7* mutants (Tanizawa *et al.* 2006). Given the suppression of the *ttx-7* defects by *egl-8* mutations, we investigated whether *egl-8* mutant animals are resistant to LiCl treatment. Treatment of wild-type animals with LiCl substantially reduced the fraction of IT behavior, while LiCl did not affect IT behavior of *egl-8(nj77)* mutants (Figure 6A). The localization of SNB-1::VENUS remained intact in LiCl-treated *egl-8(n488)* mutants unlike LiCl-treated wild-type animals (Figure 6B).

We noted that LiCl treatment shortened the body length of animals (Figure 6, C and D). This is consistent with the previous reports that lithium interferes with normal development in various organisms (Gurvich and Klein 2002). The effect of LiCl on the body size does not appear to be caused by inhibition of IMPase, because the body size of *ttx-7* mutants was normal and because LiCl treatment shortened the body size of *ttx-7* mutants (Figure 6C). In contrast to the synaptic and thermotaxis phenotypes, mutations in *egl-8* did not confer resistance to the developmental defect (Figure 6, C and D), indicating that resistance to LiCl conferred by the loss of EGL-8 function is specific to the abnormalities associated with IMPase dysfunction. These results suggest that lithium impairs synthesis of PIP_2 through inhibition of IMPase, which causes the defect in the synaptic polarity of RIA.

Discussion

The PIP_2 level in central interneurons of C. elegans is regulated by IMPase

Despite its well-known enzymatic property, the *in vivo* function of IMPase in neuronal PI metabolism has remained elusive. In this study, we show that the localization defects of synaptic proteins in IMPase *ttx-7* mutants can be suppressed by disrupting PIP_2 breakdown mediated by two membrane-associated enzymes, PLCβ EGL-8 or synaptojanin UNC-26. These results suggest that the neuronal PIP_2 level is regulated by IMPase *in vivo* and that the proper PIP_2 level is required for the synaptic polarity in a specific type of central neuron and thereby for normal behaviors.

We did not identify any other mutations in PI metabolic genes that suppress the defects of *ttx-7* mutants or cause a defect in localization of synaptic proteins similar to that in *ttx-7* mutants (Table 1). Further, the overexpression of *ppk-1*, which is known to be a major PIP_2-producing enzyme (Weinkove *et al.* 2008), had no effect on the synaptic defects of *ttx-7* mutants (Figure S4C and Table 1). These results suggest that TTX-7 and the PI metabolic enzymes tested here act in different domains of PI metabolism in RIA. Consistently, although PI is an important regulator of cell morphology (Skwarek and Boulianne 2009), the RIA morphology in *ttx-7* mutants is almost normal (Figure 2F).

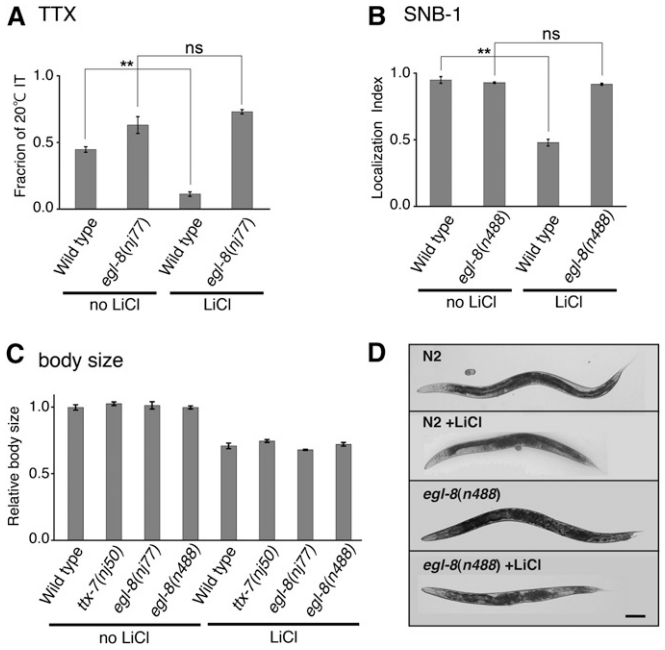

Figure 6 Exogenous application of lithium to *egl-8* mutants. (A) The effect of LiCl treatment on the individual thermotaxis assay in 20° cultivation. Lithium treatment significantly disrupted the IT behavior of wild-type animals, but not that of *egl-8(nj77)* mutants. About 20 animals were examined in more than three trials. Tukey–Kramer test was performed. (B) The localization indices of SNB-1::VENUS in the RIA neuron of animals treated with LiCl. SNB-1::VENUS in LiCl-treated wild-type animals was mislocalized to the proximal region of RIA, resulting in the lower localization index. *egl-8(n488)* mutants were completely resistant to lithium treatment. Steel–Dwass multiple comparison test was performed ($n \geq 12$ animals). (C) Body size of lithium-treated and -untreated animals in each genotype relative to lithium-untreated wild-type animals. LiCl-treated animals were smaller than untreated animals. Mutations in *egl-8* did not confer resistance in this case. $n \geq 19$ animals. (D) Lateral views of lithium-treated and -untreated adult animals captured in bright fields. Scale bar, 100 μm.

Further, a certain amount of SV proteins are transported to the presynaptic region by the PIP_2-dependent kinesin motor UNC-104 (Figure 2 and Figure 5; Klopfenstein and Vale 2004). These results suggest that the level of PI in RIA is not drastically reduced in *ttx-7* mutants and that IMPase regulates a specialized part of the entire PI metabolism in the cell to localize synaptic molecules.

PI-mediated signaling regulates the polarized localization of pre- and postsynaptic components

How does the IMPase-mediated PI signaling localize synaptic molecules? Our study showed that some portion of the SV protein SNB-1 is mislocalized in *ttx-7* mutants with a mutation in the kinesin SV transporter UNC-104 (Figure 5). Although careful interpretation is required because the *unc-104* mutation is not null, this result suggests that the mislocalization of SNB-1 is not caused merely by the defect in the movement of the transporter. As mentioned by Nonet *et al.* (1999), a defect in the endocytosis process caused by a *unc-11* mutation leads to mislocalization of SNB-1 along the membrane of neuronal processes in a *unc-104* mutant background (Nonet *et al.* 1999). However, the smooth membranous appearance of SNB-1::VENUS in *unc-11;unc-104* animals is different from the punctate appearance in *ttx-7; unc-104* animals (Figure 5A and Figure S4B). Further, the mislocalization of SNB-1::VENUS in *ttx-7;unc-104* was restricted to the proximal region of the process, while in *unc-11;unc-104* animals, SNB-1::VENUS was visible across the entire process (Figure 5A and Figure S4B), suggesting that TTX-7 and UNC-11 are involved in distinct processes.

It is possible that UNC-11-independent endocytosis is defective in *ttx-7* mutants. Margeta *et al.* (2009) showed that UNC-101, AP-1 medium subunit μ1, endocytically eliminates postsynaptic components at the presynaptic region of the RIA neuron (Margeta *et al.* 2009). Thus, we can speculate that another endocytotic machinery also functions in the PI signaling-dependent manner to eliminate presynaptic proteins such as SNB-1 at the postsynaptic region. We found that the localization of UNC-101 was disrupted in *ttx-7* mutant animals (Figure S4A). This result implies that functional localization of such endocytotic machinery is also under the control of the PI signaling.

An alternative possibility is a defect of a selective transport system. Since many synaptic components contain the PIP_2 binding domain, PIP_2 might function as a signal for synaptic components to ride on specific cargos at the Golgi apparatus. However, given that EGL-8 and UNC-26 function on the cell membrane, it is likely that the loss of TTX-7 does not significantly affect the level of PIP_2 at the Golgi apparatus.

A defect in cytoplasmic barriers might also cause the localization defects. Studies in vertebrates showed that ankyrin G- and F-actin are essential for cytoplasmic barriers to regulate protein localization in neurons (Nakada *et al.* 2003; Song *et al.* 2009). Although the loss of *unc-44*, which is the closest gene to ankyrin G in *C. elegans*, did not affect the localization of SNB-1::VENUS in RIA (Table 1), this result does not exclude the presence of such barriers.

The synaptic phenotype of *ttx-7* mutants is unique: the disruption of all examined genes related to synapse formation or polarity establishment did not cause the *ttx-7*-like defects (Table 1; Tanizawa *et al.* 2006). Thus, it is likely that the PI signaling regulated by IMPase plays a fundamental role in a novel mechanism of synaptic localization. Andreassi *et al.* (2010) showed that the mRNA of mice IMPase accumulated in the axon of sympathetic neurons, also implying an important role of IMPase in neuronal processes (Andreassi *et al.* 2010). Although technically challenging, an electron microscopy analysis will be informative to fully understand how IMPase regulates localization of synaptic molecules.

Lithium impairs PIP_2-mediated signaling through inhibition of IMPase in specific neurons

IMPase is a potent target of lithium therapy for bipolar disorder (Hallcher and Sherman 1980). It is hypothesized

that the inhibition of IMPase by lithium reduces the inositol supply, which in turn interferes with a PIP_2-mediated signaling pathway (Figure S2; Allison and Stewart 1971; Allison *et al.* 1976; Berridge *et al.* 1982, 1989; Schloesser *et al.* 2008). Indeed, a recent study using the social amoeba *Dictyostelium* showed that lithium treatment disrupts synthesis of PI species (King *et al.* 2009). However, inhibition of IMPase by lithium has never been shown to reduce neuronal PI levels *in vivo*, and studies suggesting the limited importance of IMPase in neuronal PI metabolism are accumulating (Godfrey *et al.* 1989; Batty and Downes 1994; Dixon *et al.* 1994; Schloesser *et al.* 2008; O'brien and Klein 2009). Of those, a study with mice lacking the SMIT1 gene that is required for taking up inositol from the extracellular environment (Figure 3B; Berry *et al.* 2004) showed that the loss of SMIT1 causes 92% reduction of inositol in fetal brain but does not affect PI levels. This result implies that the low concentration of inositol is sufficient to synthesize PI species. Considering that the reduction of inositol by IMPase inhibition is much more modest compared with that in the SMIT1 knockout mice, the authors claimed that the inositol depletion hypothesis is not probable (Berry *et al.* 2004). However, if the inhibition of IMPase reduces PI levels in a specific region of the nervous system and a unique metabolic module within a cell, the global measurement would not reveal the reduction of PI levels. As shown by Tanizawa *et al.* (2006), the localization defects of synaptic proteins in *ttx-7* mutants occur exclusively in the RIA neuron (Tanizawa *et al.* 2006). Further, this study showed that IMPase is involved in a specialized part of PI metabolism in the cell. Thus, inhibition of IMPase in human brain might also affect only specific types of neurons and also specific types of metabolic modules of PI metabolism in the neurons. This idea can help explain the controversial results obtained by different experimental samples.

The RIA neuron has numerous synapses in its single neurite. The high level of total synaptic activity might consume a large amount of inositol, making RIA sensitive to the IMPase inhibition. If so, neurons with a relatively large number of synapses can be a potent candidate for the target of lithium treatment in human brain.

It was shown that knockout of the IMPA1 or IMPA2 genes encoding IMPase in mice does not decrease the global level of inositol in the adult brain (Cryns *et al.* 2007, 2008; Agam *et al.* 2009), which is consistent with the result that *ttx-7* mutants does not show any defects related to the known inositol and PI-mediated signaling (Tanizawa *et al.* 2006). It is plausible that mammalian IMPase also acts in a specialized part of PI metabolism.

We also found that synaptojanin UNC-26 is linked to the PI metabolism in which IMPase and PLCβ function. Genetic studies on human patients suggested that synaptojanin 1 is also associated with bipolar disorder (Saito *et al.* 2001; Stopkova *et al.* 2004), raising an intriguing hypothesis that the metabolic module of IMPase, PLCβ, and synaptojanin at synapses is a site of lithium action.

Acknowledgments

We thank M. Nonet for pSB120; C. Rongo for CR120; M. Zhen for pJH23; P. Sengupta for *ofm-1p*::*gfp*; S. Nurrish for REW1 and KP316; K. Kimura for pKDK66; D. Weinkove for EG3361; N. Hisamoto and K. Matsumoto for *lrk-1*(*km17*) and *pld-1*(*km22*) mutant strains; *Caenorhabditis* Genetic Center and National Bioresource Project (Japan) for strains; M. Okumura for the *glr-3* promoter; A. Fire for pPD plasmid; and the members of the Mori laboratory for fruitful discussions. T.K. was supported by the Japan Society for the Promotion of Science. This work was supported by CREST, Japan Science and Technology Agency, and Grant-in-Aid for Scientific Research on Innovative Areas "Neural Diversity and Neocortical Organization" from the Ministry of Education, Culture, Sports, Science and Technology (MEXT) of Japan to IM.

Literature Cited

Agam, G., Y. Bersudsky, G. T. Berry, D. Moechars, Y. Lavi-Avnon *et al.*, 2009 Knockout mice in understanding the mechanism of action of lithium. Biochem. Soc. Trans. 37: 1121–1125.

Allison, J. H., and M. A. Stewart, 1971 Reduced brain inositol in lithium-treated rats. Nat. New Biol. 233: 267–268.

Allison, J. H., M. E. Blisner, W. H. Holland, P. P. Hipps, and W. R. Sherman, 1976 Increased brain *myo*-inositol 1-phosphate in lithium-treated rats. Biochem. Biophys. Res. Commun. 71: 664–670.

Andreassi, C., C. Zimmermann, R. Mitter, S. Fusco, S. De Vita *et al.*, 2010 An NGF-responsive element targets *myo*-inositol monophosphatase-1 mRNA to sympathetic neuron axons. Nat. Neurosci. 13: 291–301.

Arimura, N., and K. Kaibuchi, 2005 Key regulators in neuronal polarity. Neuron 48: 881–884.

Arimura, N., and K. Kaibuchi, 2007 Neuronal polarity: from extracellular signals to intracellular mechanisms. Nat. Rev. Neurosci. 8: 194–205.

Batty, I. H., and C. P. Downes, 1994 The inhibition of phosphoinositide synthesis and muscarinic-receptor-mediated phospholipase C activity by Li^+ as secondary, selective, consequences of inositol depletion in 1321N1 cells. Biochem. J. 297(3): 529–537.

Berridge, M. J., C. P. Downes, and M. R. Hanley, 1982 Lithium amplifies agonist-dependent phosphatidylinositol responses in brain and salivary glands. Biochem. J. 206: 587–595.

Berridge, M. J., C. P. Downes, and M. R. Hanley, 1989 Neural and developmental actions of lithium: a unifying hypothesis. Cell 59: 411–419.

Berry, G. T., R. Buccafusca, J. J. Greer, and E. Eccleston, 2004 Phosphoinositide deficiency due to inositol depletion is not a mechanism of lithium action in brain. Mol. Genet. Metab. 82: 87–92.

Brenner, S., 1974 The genetics of *Caenorhabditis elegans*. Genetics 77: 71–94.

Cade, J. F. J., 1949 Lithium salts in the treatment of psychotic excitement. Med. J. Aust. 2: 349–352.

Cremona, O., G. Di Paolo, M. R. Wenk, A. Lüthi, W. T. Kim *et al.*, 1999 Essential role of phosphoinositide metabolism in synaptic vesicle recycling. Cell 99: 179–188.

Cryns, K., A. Shamir, J. Shapiro, G. Daneels, I. Goris *et al.*, 2007 Lack of lithium-like behavioral and molecular effects in IMPA2 knockout mice. Neuropsychopharmacology 32: 881–891.

Cryns, K., A. Shamir, N. Van Acker, I. Levi, G. Daneels *et al.*, 2008 IMPA1 is essential for embryonic development and lithium-like pilocarpine sensitivity. Neuropsychopharmacology 33: 674–684.

De Matteis, M., A. Godi, and D. Corda, 2002 Phosphoinositides and the golgi complex. Curr. Opin. Cell Biol. 14: 434–447.

Di Paolo, G., and P. De Camilli, 2006 Phosphoinositides in cell regulation and membrane dynamics. Nature 443: 651–657.

Dixon, J. F., G. V. Los, and L. E. Hokin, 1994 Lithium stimulates glutamate "release" and inositol 1,4,5-trisphosphate accumulation via activation of the *N*-methyl-D-aspartate receptor in monkey and mouse cerebral cortex slices. Proc. Natl. Acad. Sci. USA 91: 8358–8362.

Dwyer, N. D., C. E. Adler, J. G. Crump, N. D. L'Etoile, and C. I. Bargmann, 2001 Polarized dendritic transport and the AP-1 mu1 clathrin adaptor UNC-101 localize odorant receptors to olfactory cilia. Neuron 31: 277–287.

Godfrey, P. P., S. J. McClue, A. M. White, A. J. Wood, and D. G. Grahame-Smith, 1989 Subacute and chronic in vivo lithium treatment inhibits agonist- and sodium fluoride-stimulated inositol phosphate production in rat cortex. J. Neurochem. 52: 498–506.

Gotta, M., M. C. Abraham, and J. Ahringer, 2001 CDC-42 controls early cell polarity and spindle orientation in *C. elegans*. Curr. Biol. 11: 482–488.

Gurvich, N., and P. S. Klein, 2002 Lithium and valproic acid: parallels and contrasts in diverse signaling contexts. Pharmacol. Ther. 96: 45–66.

Hall, D. H., and E. M. Hedgecock, 1991 Kinesin-related gene *unc-104* is required for axonal transport of synaptic vesicles in *C. elegans*. Cell 65: 837–847.

Hallcher, L. M., and W. R. Sherman, 1980 The effects of lithium ion and other agents on the activity of *myo*-inositol-1-phosphatase from bovine brain. J. Biol. Chem. 255: 10896–10901.

Harris, T. W., E. Hartwieg, H. R. Horvitz, and E. M. Jorgensen, 2000 Mutations in synaptojanin disrupt synaptic vesicle recycling. J. Cell Biol. 150: 589–600.

Hedgecock, E. M., and R. L. Russell, 1975 Normal and mutant thermotaxis in the nematode *Caenorhabditis elegans*. Proc. Natl. Acad. Sci. USA 72: 4061–4065.

Hedgepeth, C. M., L. J. Conrad, J. Zhang, H. C. Huang, V. M. Lee *et al.*, 1997 Activation of the Wnt signaling pathway: a molecular mechanism for lithium action. Dev. Biol. 185: 82–91.

Ito, H., H. Inada, and I. Mori, 2006 Quantitative analysis of thermotaxis in the nematode *Caenorhabditis elegans*. J. Neurosci. Methods 154: 45–52.

Jurado, P., E. Kodama, Y. Tanizawa, and I. Mori, 2010 Distinct thermal migration behaviors in response to different thermal gradients in *Caenorhabditis elegans*. Genes Brain Behav. 9: 120–127.

Kay, A. J., and C. P. Hunter, 2001 CDC-42 regulates PAR protein localization and function to control cellular and embryonic polarity in *C. elegans*. Curr. Biol. 11: 474–481.

King, J. S., R. Teo, J. Ryves, J. V. Reddy, O. Peters *et al.*, 2009 The mood stabiliser lithium suppresses PIP_3 signalling in Dictyostelium and human cells. Dis. Model Mech. 2: 306–312.

Klopfenstein, D. R., and R. D. Vale, 2004 The lipid binding pleckstrin homology domain in UNC-104 kinesin is necessary for synaptic vesicle transport in *Caenorhabditis elegans*. Mol. Biol. Cell 15: 3729–3739.

Komatsu, H., I. Mori, J. S. Rhee, N. Akaike, and Y. Ohshima, 1996 Mutations in a cyclic nucleotide-gated channel lead to abnormal thermosensation and chemosensation in *C. elegans*. Neuron 17: 707–718.

Lackner, M. R., S. J. Nurrish, and J. M. Kaplan, 1999 Facilitation of synaptic transmission by EGL-30 Gqalpha and EGL-8 PLCbeta: DAG binding to UNC-13 is required to stimulate acetylcholine release. Neuron 24: 335–346.

Lee, Y.-S., S. Mulugu, J. D. York, and E. K. O'Shea, 2007 Regulation of a cyclin-CDK-CDK inhibitor complex by inositol pyrophosphates. Science 316: 109–112.

Luo, L., D. A. Clark, D. Biron, L. Mahadevan, and A. D. T. Samuel, 2006 Sensorimotor control during isothermal tracking in *Caenorhabditis elegans*. J. Exp. Biol. 209: 4652–4662.

Machado-Vieira, R., H. K. Manji, J. Zarate, and A. Carlos, 2009 The role of lithium in the treatment of bipolar disorder: convergent evidence for neurotrophic effects as a unifying hypothesis. Bipolar Disord. 11(Suppl. 2): 92–109.

Margeta, M. A., G. J. Wang, and K. Shen, 2009 Clathrin adaptor AP-1 complex excludes multiple postsynaptic receptors from axons in *C. elegans*. Proc. Natl. Acad. Sci. USA 106: 1632–1637.

Maslanski, J. A., L. Leshko, and W. B. Busa, 1992 Lithium-sensitive production of inositol phosphates during amphibian embryonic mesoderm induction. Science 256: 243–245.

Mello, C., J. Kramer, D. Stinchcomb, and V. Ambros, 1991 Efficient gene transfer in *C. elegans*: extrachromosomal maintenance and inte-gration of transforming sequences. EMBO J. 10: 3959–3970.

Miller, K. G., M. D. Emerson, and J. B. Rand, 1999 Goalpha and diacylglycerol kinase negatively regulate the Gqalpha pathway in *C. elegans*. Neuron 24: 323–333.

Mohri, A., E. Kodama, K. D. Kimura, M. Koike, T. Mizuno *et al.*, 2005 Genetic control of temperature preference in the nematode *Caenorhabditis elegans*. Genetics 169: 1437–1450.

Mori, I., and Y. Ohshima, 1995 Neural regulation of thermotaxis in *Caenorhabditis elegans*. Nature 376: 344–348.

Nakada, C., K. Ritchie, Y. Oba, M. Nakamura, Y. Hotta *et al.*, 2003 Accumulation of anchored proteins forms membrane diffusion barriers during neuronal polarization. Nat. Cell Biol. 5: 626–632.

Nicot, A.-S., H. Fares, B. Payrastre, A. D. Chisholm, M. Labouesse *et al.*, 2006 The phosphoinositide kinase PIKfyve/Fab1p regulates terminal lysosome maturation in *Caenorhabditis elegans*. Mol. Biol. Cell 17: 3062–3074.

Nonet, M. L., A. M. Holgado, F. Brewer, C. J. Serpe, B. A. Norbeck *et al.*, 1999 UNC-11, a *Caenorhabditis elegans* AP180 homologue, regulates the size and protein composition of synaptic vesicles. Mol. Biol. Cell 10: 2343–2360.

O'Brien, W. T., and P. S. Klein, 2009 Validating GSK3 as an in vivo target of lithium action. Biochem. Soc. Trans. 37: 1133–1138.

O'Donnell, T., S. Rotzinger, T. T. Nakashima, C. C. Hanstock, M. Ulrich *et al.*, 2000 Chronic lithium and sodium valproate both decrease the concentration of *myo*-inositol and increase the concentration of inositol monophosphates in rat brain. Brain Res. 880: 84–91.

Odom, A. R., A. Stahlberg, S. R. Wente, and J. D. York, 2000 A role for nuclear inositol 1,4,5-trisphosphate kinase in transcriptional control. Science 287: 2026–2029.

Ohnishi, T., A. Watanabe, H. Ohba, Y. Iwayama, M. Maekawa *et al.*, 2010 Behavioral analyses of transgenic mice harboring bipolar disorder candidate genes, IMPA1 and IMPA2. Neurosci. Res. 67: 86–94.

Okochi, Y., K. D. Kimura, A. Ohta, and I. Mori, 2005 Diverse regulation of sensory signaling by *C. elegans* nPKC-epsilon/eta TTX-4. EMBO J. 24: 2127–2137.

Otsuka, A. J., A. Jeyaprakash, J. Garcia-Anoveros, L. Z. Tang, G. Fisk *et al.*, 1991 The *C. elegans unc-104* gene encodes a putative kinesin heavy chain-like protein. Neuron 6: 113–122.

Otsuka, A. J., R. Franco, B. Yang, K. H. Shim, L. Z. Tang *et al.*, 1995 An ankyrin-related gene (*unc-44*) is necessary for proper axonal guidance in *Caenorhabditis elegans*. J. Cell Biol. 129: 1081–1092.

Ryu, W. S., and A. D. T. Samuel, 2002 Thermotaxis in *Caenorhabditis elegans* analyzed by measuring responses to defined thermal stimuli. J. Neurosci. 22: 5727–5733.

Saito, T., F. Guan, D. F. Papolos, S. Lau, M. Klein *et al.*, 2001 Mutation analysis of SYNJ1: a possible candidate gene for chromosome 21q22-linked bipolar disorder. Mol. Psychiatry 6: 387–395.

Sakaguchi-Nakashima, A., J. Y. Meir, Y. Jin, K. Matsumoto, and N. Hisamoto, 2007 LRK-1, a *C. elegans* PARK8-related kinase, regulates axonal-dendritic polarity of SV proteins. Curr. Biol. 17: 592–598.

Sawa, M., and T. Takenawa, 2006 *Caenorhabditis elegans* WASP-interacting protein homologue WIP-1 is involved in morphogenesis through maintenance of WSP-1 protein levels. Biochem. Biophys. Res. Commun. 340: 709–717.

Sawa, M., S. Suetsugu, A. Sugimoto, H. Miki, M. Yamamoto *et al.*, 2003 Essential role of the *C. elegans* Arp2/3 complex in cell migration during ventral enclosure. J. Cell Sci. 116: 1505–1518.

Schloesser, R. J., J. Huang, P. S. Klein, and H. K. Manji, 2008 Cellular plasticity cascades in the pathophysiology and treatment of bipolar disorder. Neuropsychopharmacology 33: 110–133.

Seeds, A. M., R. J. Bastidas, and J. D. York, 2005 Molecular definition of a novel inositol polyphosphate metabolic pathway initiated by inositol 1,4,5-trisphosphate 3-kinase activity in *Saccharomyces cerevisiae*. J. Biol. Chem. 280: 27654–27661.

Shaldubina, A., S. Ju, D. L. Vaden, D. Ding, R. H. Belmaker *et al.*, 2002 Epi-inositol regulates expression of the yeast INO1 gene encoding inositol-1-P synthase. Mol. Psychiatry 7: 174–180.

Skwarek, L. C., and G. L. Boulianne, 2009 Great expectations for PIP: phosphoinositides as regulators of signaling during development and disease. Dev. Cell 16: 12–20.

Song, A.-H., D. Wang, G. Chen, Y. Li, J. Luo *et al.*, 2009 A selective filter for cytoplasmic transport at the axon initial segment. Cell 136: 1148–1160.

Stephens, L. R., K. T. Hughes, and R. F. Irvine, 1991 Pathway of phosphatidylinositol(3,4,5)-trisphosphate synthesis in activated neutrophils. Nature 351: 33–39.

Stopkova, P., J. Vevera, I. Paclt, I. Zukov, and H. M. Lachman, 2004 Analysis of SYNJ1, a candidate gene for 21q22 linked bipolar disorder: a replication study. Psychiatry Res. 127: 157–161.

Takenawa, T., and S. Suetsugu, 2007 The WASP-WAVE protein network: connecting the membrane to the cytoskeleton. Nat. Rev. Mol. Cell Biol. 8: 37–48.

Tanizawa, Y., A. Kuhara, H. Inada, E. Kodama, T. Mizuno *et al.*, 2006 Inositol monophosphatase regulates localization of synaptic components and behavior in the mature nervous system of *C. elegans*. Genes Dev. 20: 3296–3310.

Tsuboi, D., T. Hikita, H. Qadota, M. Amano, and K. Kaibuchi, 2005 Regulatory machinery of UNC-33 Ce-CRMP localization in neurites during neuronal development in *Caenorhabditis elegans*. J. Neurochem. 95: 1629–1641.

Weinkove, D., M. Bastiani, T. A. M. Chessa, D. Joshi, L. Hauth *et al.*, 2008 Overexpression of PPK-1, the *Caenorhabditis elegans* Type I PIP kinase, inhibits growth cone collapse in the developing nervous system and causes axonal degeneration in adults. Dev. Biol. 313: 384–397.

White, J. G., E. Southgate, J. N. Thomson, and S. Brenner, 1986 The structure of the nervous system of the nematode *Caenorhabditis elegans*. Philos. Trans. R. Soc. Lond. B Biol. Sci. 314: 1–340.

Whiteford, C. C., C. A. Brearley, and E. T. Ulug, 1997 Phosphatidylinositol 3,5-bisphosphate defines a novel PI 3-kinase pathway in resting mouse fibroblasts. Biochem. J. 323(3): 597–601.

Wicks, S. R., R. T. Yeh, W. R. Gish, R. H. Waterston, and R. H. Plasterk, 2001 Rapid gene mapping in *Caenorhabditis elegans* using a high density polymorphism map. Nat. Genet. 28: 160–164.

Yeh, E., T. Kawano, R. M. Weimer, J.-L. Bessereau, and M. Zhen, 2005 Identification of genes involved in synaptogenesis using a fluorescent active zone marker in *Caenorhabditis elegans*. J. Neurosci. 25: 3833–3841.

Communicating editor: K. Kemphues

GENETICS

Supporting Information
http://www.genetics.org/content/suppl/2012/03/23/genetics.111.137844.DC1

Synaptic Polarity Depends on Phosphatidylinositol Signaling Regulated by *myo*-Inositol Monophosphatase in *Caenorhabditis elegans*

Tsubasa Kimata, Yoshinori Tanizawa, Yoko Can, Shingo Ikeda, Atsushi Kuhara, and Ikue Mori

DOI: 10.1534/genetics.111.137844

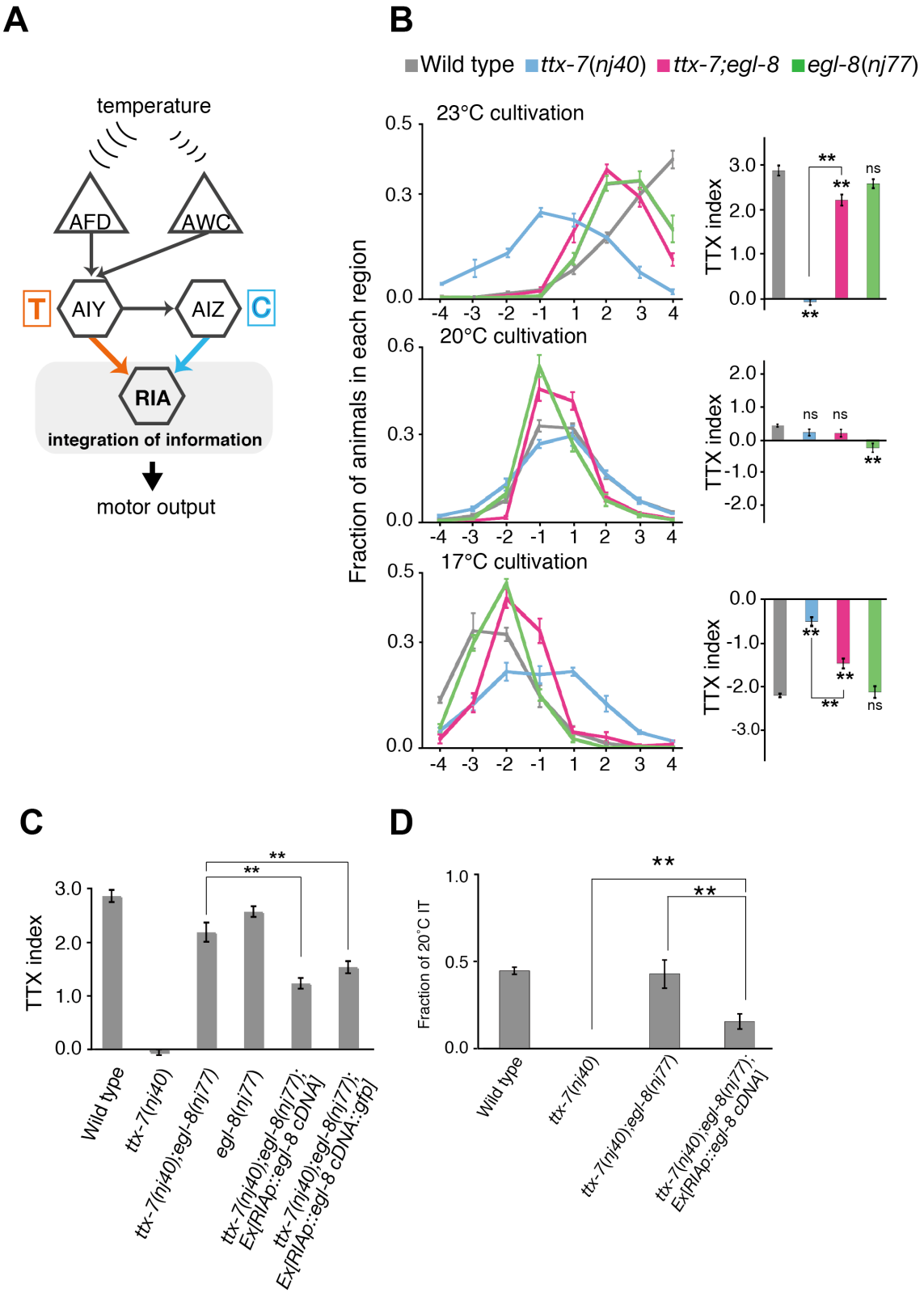

Figure S1 Thermotaxis behavior of *ttx-7*(*nj40*);*egl-8*(*nj77*) mutants (**A**) The neural circuit for thermotaxis behavior. Temperature information sensed by AFD and AWC sensory neurons is transmitted to AIY, AIZ and RIA interneurons. RIA neuron is assumed to integrate thermophilic drive conveyed from AIY neuron (designated as "T") and cryophilic drive from AIZ neuron (designated as "C") and to regulate downstream motor neurons. (**B**) Distributions and TTX indices of wild-type animals, *ttx-7*(*nj40*), *ttx-7*(*nj40*);*egl-8*(*nj77*), and *egl-8*(*nj77*) mutants cultivated at 17˚, 20˚ and 23˚. The marks on the bars

of each genotype indicate for comparisons with wild type. The marks on the lines represent for comparisons between indicated genotypes. Tukey–Kramer tests was performed (n ≥ 4 assays). (**C**) RIA specific rescue experiments for *ttx-7*(*nj40*);*egl-8*(*nj77*) mutants cultivated at 23˚ using the population thermotaxis assay. Either the expression of *egl-8* cDNA or *egl-8* cDNA::*gfp* in RIA neuron of *ttx-7*(*nj40*);*egl-8*(*nj77*) mutants partially but significantly rescued the suppression of the thermotaxis defect. Tukey–Kramer test was performed (n ≥ 4 assays). (**D**) Expressing *egl-8* cDNA specifically in RIA reduced the fraction of IT behavior in *ttx-7(nj40);egl-8(nj77)* double mutants. About 20 animals cultivated at 20˚ were examined in more than three trials, which were compared in ANOVA.

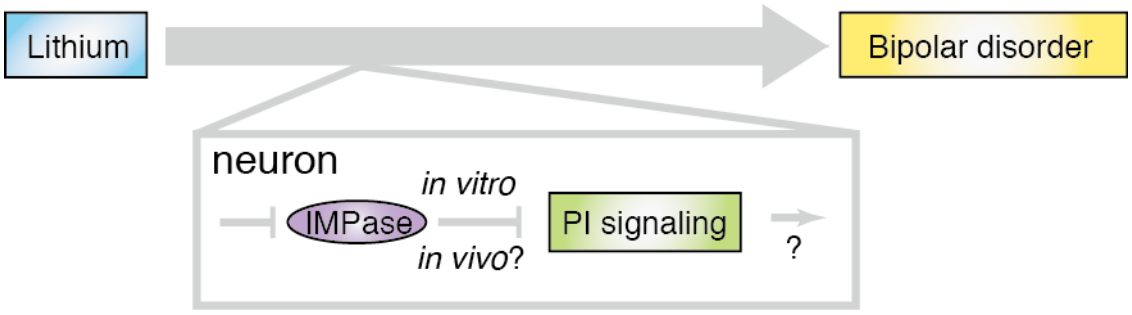

Figure S2 The inositol depletion hypothesis. The hypothesis explains that lithium exerts its effect on bipolar disorder via inhibition of IMPase. The inhibition of IMPase assumed to interfere with neuronal PI signaling but it has never been proven in vivo.

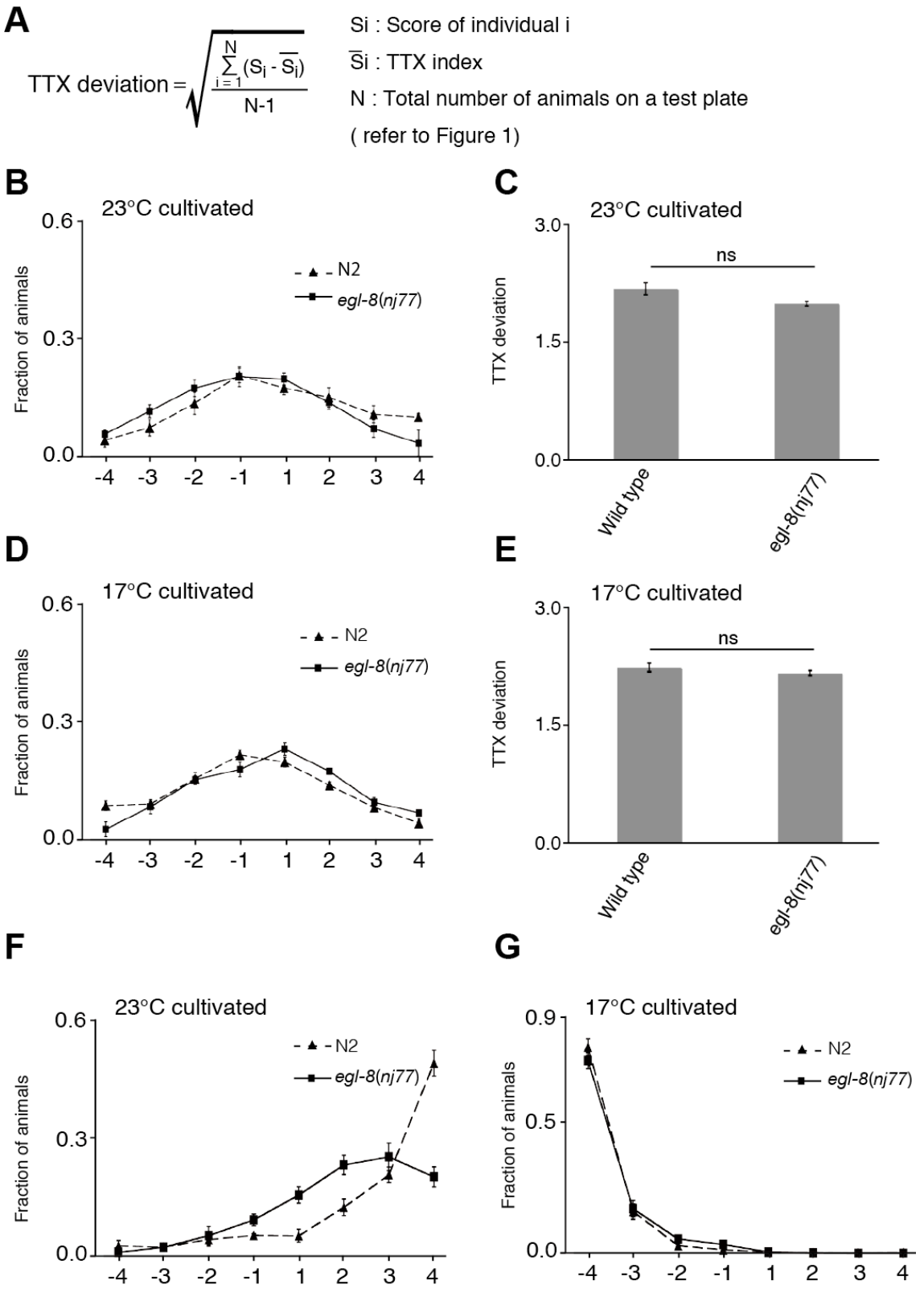

Figure S3 Thermotaxis behavior of *egl-8*(*nj77*) mutants. (**A**) The equation for calculating the TTX deviation. (**B and D**) Distributions of wild-type and *egl-8*(*nj77*) mutants on TTX plate without the temperature gradient (n ≥ 4 assays). Animals cultivated at 23˚ (B) or 17˚ (D) were placed at the center of the plate and left for 60 min at 20˚. (**C and E**) TTX deviations of

wild type and *egl-8*(*nj77*) mutants cultivated at 23˚ (C) and 17˚ (E). Although the TTX deviation of *egl-8* mutants was slightly lower than that of wild-type animals, the difference was not statistically significant. *t*-test was applied (n ≥ 4 assays). (**F and G**) Animals cultivated at 23˚ (F) or 17˚ (G) were assayed in the population thermotaxis assay for 120 min (n ≥ 4 assays). In contrast to the 60 min assay, *egl-8*(*nj77*) mutants cultivated at 17˚ migrated to the cultivation temperature as comparable to wild-type animals, but they did not at 23˚.

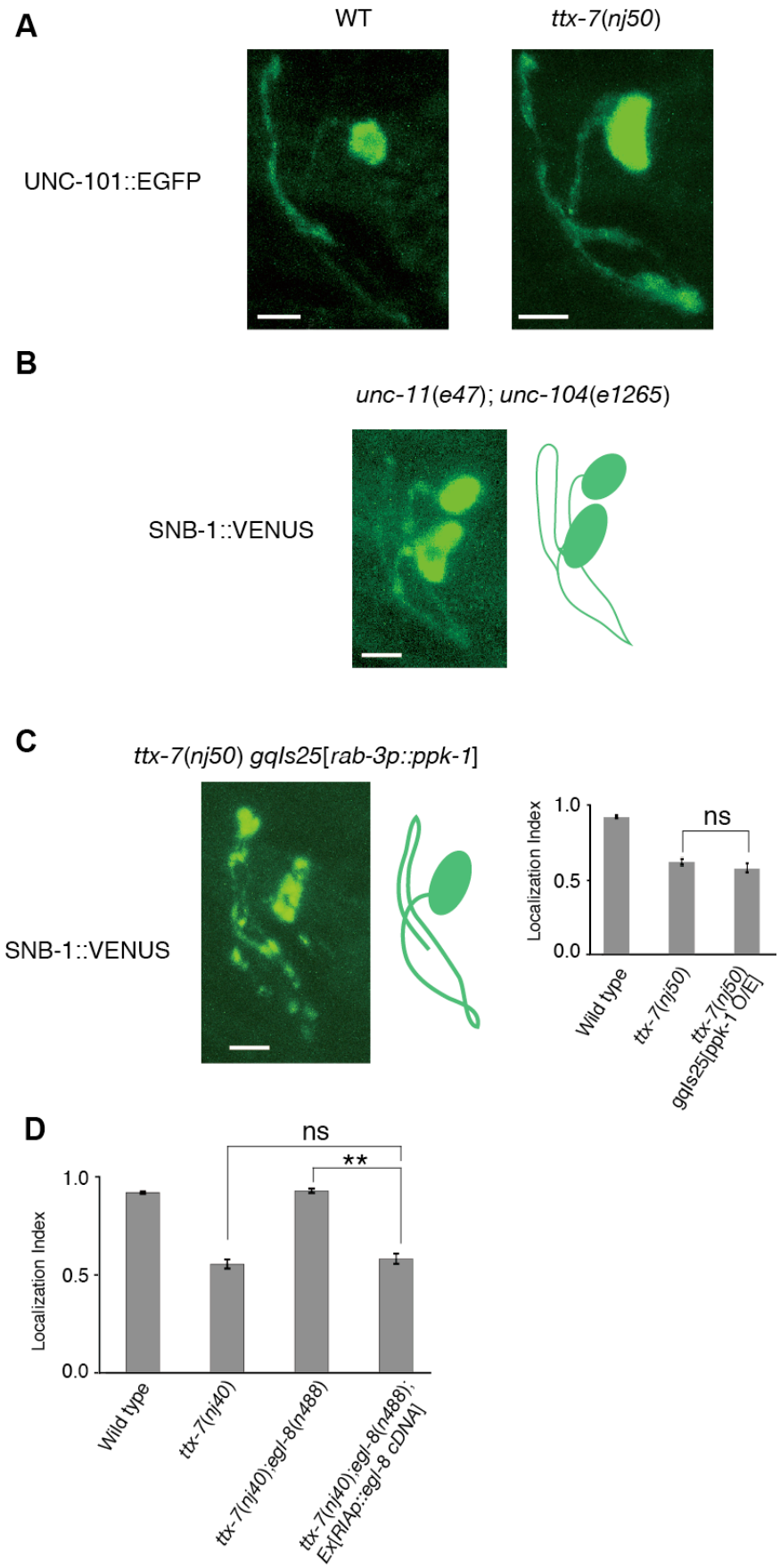

Figure S4 Localizations of synaptic components in RIA neuron. (**A**) The localization of UNC-101::GFP in RIA neuron. As described in Margeta et al. (2009), UNC-101::GFP was exclusively localized to the presynaptic region in wild-type animals. It

was mislocalized to the proximal region of the process in *ttx-7*(*nj50*) mutants. (**B**) The localization of SNB-1::VENUS in *unc-11*(*e47*);*unc-104*(*e1265*) double mutants. The fluorescence of SNB-1::VENUS was quite dim but observed in the entire process of RIA neuron. Scale bar, 5μm. (**C**) The representative image of the localization of SNB-1::VENUS in *ttx-7*(*nj50*) *gqIs25*[*rab-3p::ppk-1*] mutants and the localization indices of SNB-1::VENUS in each genotype. The overexpression of *ppk-1* gene did not suppress the localization defect in *ttx-7* mutants. Steel-Dwass multiple comparison test was performed (n ≥ 8 animals). Scale bar, 5μm. (**D**) RIA-specific expression of *egl-8* cDNA rescued the suppresion of the SNB-1-localization defect by *egl-8*(*n488*) mutation. Steel-Dwass multiple comparison test was performed (n ≥ 15 animals).